2023 IEEE International Conference on Robotics and Automation (ICRA 2023)
May 29 - June 2, 2023. London, UK

Efficient Planar Pose Estimation via UWB Measurements

Haodong Jiang[1,2], Wentao Wang[3], Yuan Shen[4], Xinghan Li[3],
Xiaoqiang Ren[5], Biqiang Mu[6], and Junfeng Wu[2,1]

***Abstract*— State estimation is an essential part of autonomous systems. Integrating the Ultra-Wideband (UWB) technique has been shown to correct the long-term estimation drift and bypass the complexity of loop closure detection. However, few works on robotics treat UWB as a stand-alone state estimation solution. The primary purpose of this work is to investigate planar pose estimation using only UWB range measurements. We prove the excellent property of a two-step scheme, which says we can refine a consistent estimator to be asymptotically efficient by one step of Gauss-Newton iteration. Grounded on this result, we design the GN-ULS estimator, which reduces the computation time significantly compared to previous methods and presents the possibility of using only UWB for real-time state estimation.**

I. INTRODUCTION

A. Background

State estimation is a fundamental prerequisite for an intelligent mobile robot to realize obstacle avoidance and path-planning tasks. In recent years, significant efforts have been devoted to achieving high-performance and real-time state estimation using onboard sensors such as IMU, cameras, and lidars. However, these methods confront issues such as long-term drift [1] and low robustness in geometrically degenerated environments [2]. To overcome the above-mentioned challenges, we can integrate external information such as GPS in state estimation [3].

Ultra-Wideband (UWB) is a radio technology that is robust to multi-path effect and can provide precise TOA or TDOA measurements [4]. UWB is traditionally used for localization [5]–[9], while many recent works [10]–[13] integrate UWB to realize drift-free state estimation in GPS-denied environments, few works on robotics investigate using UWB independently for pose estimation.

This work considers estimating a robot's pose via only UWB range measurements obtained with a symmetric two-way TOA measuring technique. We focus on the planar case as shown in Fig. 1, which has many critical applications

[1]: Shenzhen Institute of Artificial Intelligence and Robotics for Society (AIRS), haodongjiang@link.cuhk.edu.cn. [2]: School of Data Science, the Chinese University of HongKong, Shenzhen, P. R. China, junfengwu@cuhk.edu.cn. [3]: College of Control Science and Engineering and the State Key Laboratory of Industrial Control Technology, Zhejiang University, Hangzhou, P. R. China, {wwt1999,11832014}@zju.edu.cn. [4]: School of Electronic and Optical Engineering, Nanjing University of Science and Technology, Nanjing, P. R. China, syuan@njust.edu.cn. [5]: School of Mechatronic Engineering and Automation, Shanghai University, Shanghai, P. R. China, xqren@shu.edu.cn. [6]: Key Laboratory of Systems and Control, Institute of Systems Science, Academy of Mathematics and Systems Science, Chinese Academy of Sciences, Beijing, P. R. China, bqmu@amss.ac.cn

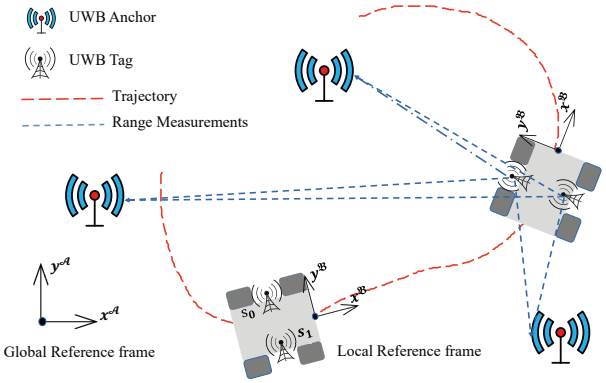

Fig. 1: Planar Pose Estimation via UWB Measurements

such as search and rescue robots [14] and indoor service robots [15]. We recognize it as the **Rigid Body Localization (RBL)** problem in the signal processing community.

Through the literature review, we find that the pose estimators' statistical efficiency has not been well studied, and the estimators' computational complexity requires further reduction to realize real-time estimation. In this work, we adopt a two-step scheme and develop a closed-form estimator, which is asymptotically efficient under mild conditions related to anchor geometry, and significantly reduces computation time. We also conduct simulations and experiments to demonstrate our method's statistical and computational efficiency.

B. Related Work on Planar Rigid Body Localization

The maximum likelihood (**ML**) formulation of RBL under i.i.d Gaussian noise assumption is a constrained weighted least squares (LS) problem (2). However, the ML estimate is difficult to obtain due to the nonconvexity and nonlinearity of (2). A common practice is to apply the least squares methodology to the squared range measurements and formulate the squared least squares (**SLS**) problem (6).

As far as we know, the work [16] is the first to formulate the RBL problem, which proposes to modify the **SLS** problem by projecting the squared measurements onto the null space of unit vectors. This operation eliminates the quadratic term and makes the problem linear, and the idea is followed by the work [17] and our work. We term the resulting formulation (7) projected squared least squares (**PSLS**). Based on **PSLS**, the work [16] solves a weighted orthogonal Procrustes problem by Gauss-Newton algorithms and obtains the initial value from simpler problems with closed-form solutions. The work [16] also derives the unitarily constrained Cramer-Rao lower bound (CRLB). The work [17] harnesses the structure of the rotation matrix and formulates a generalized trust region subproblem (GTRS), and the solution is refined on the

linearized **SLS** problem. The work [18] uses semidefinite relaxation and formulate **SLS** as a semidefinite program (SDP). The solution is refined by one step of Gauss-Newton iteration on the **ML** problem.

To sum up, the ML estimate for the planar RBL problem is difficult to obtain. Previous works turn to the **SLS** problem and use different techniques to make the problem linear. However, earlier studies do not rigorously evaluate the proposed estimators' deviation from the ML estimator or their statistical efficiency. Considering the growing interest in provably optimal state inference [19], we believe these topics deserve careful study. The theoretical results also motivate the design of a faster optimal estimator.

C. Contributions

We summarize our contributions as follows:

(i) We design a closed-form planar pose estimator using only UWB range measurements, which has $O(n)$ computational complexity and provably converges to the ML estimator as the measurement number n increases. Given the high sampling rate of practical UWB systems [20], our work can play a valuable role in applications.

(ii) We propose mild conditions related to anchor geometry, under which the ML estimator, therefore our method is asymptotically efficient, i.e., the estimate can converge to the true pose with minimum variance.

(iii) We conduct experiments in an indoor environment and elaborate on the data preprocessing procedure. The dataset and code are available on our website[1].

We organize the paper as follows. Section II gives formulations of the planar RBL problem. Section III develops the **GN-ULS** estimator in two steps. Section IV gives conditions under which the ML estimator, therefore the **GN-ULS** estimator, is asymptotically efficient. Section V compare different estimators via various simulations. Section V introduces data collection and discusses experiments on static and dynamic datasets. Section VII concludes the paper and discusses future works.

Notations: All vectors are column vectors and denoted by bold, lower case letters; matrices are denoted by bold, upper case letters; reference frames are denoted with $\mathscr{A},\mathscr{B},\mathscr{C}$. $\mathrm{vec}(\mathbf{A})$ is a column vector obtained by stacking the columns of matrix $\mathbf{A}$. $\mathrm{Null}(\mathbf{A})$ is the null space of $\mathbf{A}$. We use $\mathbf{I},\mathbf{1},\mathbf{0}$ to denote identity matrices, unit vectors or matrices, and zero vectors or matrices. The symbol $\odot$ represents the Hadamard product and $\otimes$ the Kronecker product. For a list of vectors, we use the tuple notation $(\mathbf{v_1},\mathbf{v_2}\dots,\mathbf{v_n})$ for $[\mathbf{v_1}^\top,\mathbf{v_2}^\top\dots,\mathbf{v_n}^\top]^\top$. We use the notation $\mathbf{a}^o$ for the true value of an unknown variable $\mathbf{a}$. We use the notation $O_p(\mathbf{1})$ for vectors or matrices whose entries are $O_p(1)$, i.e., stochastically bounded. We use the notation $o_p(\mathbf{1})$ for vectors or matrices whose entries are $o_p(1)$, i.e., convergent in probability towards zero..

[1]https://github.com/SLAMLab-CUHKSZ/Efficient-Pose-Estimation-via-UWB-measurements

II. Planar Rigid Body Localization

A. Range Measurement Model

Let $\mathscr{A}$ be the global frame, and let $\mathscr{B}$ be the local frame of the rigid body. The z-axes of $\mathscr{A}$ and $\mathscr{B}$ are aligned.

Let $\mathbf{a}_m^{\mathscr{A}} \in \mathbb{R}^2, m \in \{1,\dots,M\}$ be the planar coordinates of M anchors in $\mathscr{A}$. Let $\mathbf{s}_i^{\mathscr{B}} \in \mathbb{R}^2, i \in \{1,\dots,N\}$ be the planar coordinates in $\mathscr{B}$ of N tags fixed on the rigid boy. The planar pose of $\mathscr{B}$ with respect to $\mathscr{A}$ can be represented by a rotation matrix $\mathbf{R}^o \in \mathrm{SO}(2)$ and a position vector $\mathbf{t}^o \in \mathbb{R}^2$. Each anchor can range with each tag repeatedly. For the brevity of formulation, we consider repeatedly ranging for T times equivalent to deploying T anchors on the same site. In total, we have $M_T \triangleq MT$ anchors and $n = NM_T$ measurements.

We denote by d_{im} the distance measurement betweem the m-th anchor and the i-th tag, denote by Δh_{im} the height difference between the m-th anchor and the i-th tag. The distance measurement model is as follows:

$$d_{im} = \sqrt{\|\mathbf{a}_m^{\mathscr{A}} - \mathbf{R}^o\mathbf{s}_i^{\mathscr{B}} - \mathbf{t}^o\|^2 + (\Delta h_{im})^2} + r_{im} \tag{1}$$

where r_{im} is the additive measurement noise.

The RBL problem is formulated as follows: given $\mathbf{a}_m^{\mathscr{A}}$, $\mathbf{s}_i^{\mathscr{B}}$, Δh_{im} and the distance measurements d_{im}, estimate the pose of the rigid body, i.e., the rotation $\mathbf{R}^o$ and the position $\mathbf{t}^o$.

B. Assumptions

We make the following assumptions:

Assumption 1: Anchors and tags are on the same height.

Remark 1: We assume $\Delta h_{im} = 0$ for simplicity, modification for $\Delta h_{im} \neq 0$ is straightforward and detailed in [21].

Assumption 2: r_{im}'s are i.i.d Gaussian noises with zero mean, finite and known standard deviation $\sigma_{im} > 0$.

Assumption 3: The sample distribution F_m of the sequence $\mathbf{a}_1^{\mathscr{A}}, \mathbf{a}_2^{\mathscr{A}}, \dots$ converges to some distribution F_μ.

Example 1: Suppose $\mathbf{a}_m^{\mathscr{A}}$'s are independent samples from distribution function F_μ, F_m converges to F_μ as M increases.

Example 2: As the number T of repeated ranging increases, F_m converges to F_μ. Denote the measure induced by F_μ as μ, we have $\mu(\mathbf{a}_m^{\mathscr{A}}) = \frac{1}{M}$ for $m = 1,\dots,M$.

Assumption 4: At least three non-colinear anchors exist, and at least two tags non-colinear with the origin $O^{\mathscr{B}}$ of the local reference frame.

Remark 2: The necessary and sufficient condition for the planar pose to be observable requires at least three non-colinear anchors and at least two tags [21]. Under specific constraints, the required sensors can be further reduced, such as in work [22]. We make a slightly stronger assumption in this paper to ease the proof of Lemma 1.

Assumption 5: Consider the limit measure μ in Assumption 3, there does not exist any line $\mathscr{L}$ such that $\mu(\mathscr{L}) = 1$.

C. Maximum Likelihood Formulation

The ML estimates $\hat{\mathbf{R}}_{\mathrm{ML}}, \hat{\mathbf{t}}_{\mathrm{ML}}$ of the planar RBL problem are the solution to the following optimization problem:

$$\textbf{(ML)} \quad \min_{\mathbf{R},\mathbf{t}} \quad \sum_{i=1}^{N}\sum_{m=1}^{M_T} \frac{(d_{im} - \|\mathbf{a}_m^{\mathscr{A}} - \mathbf{R}\mathbf{s}_i^{\mathscr{B}} - \mathbf{t}\|)^2}{\sigma_{im}^2} \tag{2a}$$

$$\text{s.t.} \quad \mathbf{R} \in \mathrm{SO}(2),\ \mathbf{t} \in \mathbb{R}^2, \tag{2b}$$

D. Squared Least Squares Formulation

The **ML** formulation is non-linear, non-convex, and difficult to solve. We square both sides of (1) and have:

$$d_{im}^2 = (\|\mathbf{a}_m^{\mathscr{A}} - \mathbf{R}\mathbf{s}_i^{\mathscr{B}} - \mathbf{t}\| + r_{im})^2 \tag{3a}$$

$$= \|\mathbf{a}_m^{\mathscr{A}}\|^2 - 2\mathbf{a}_m^{\mathscr{A}\top}(\mathbf{R}\mathbf{s}_i^{\mathscr{B}} + \mathbf{t}) + \|\mathbf{R}\mathbf{s}_i^{\mathscr{B}} + \mathbf{t}\|^2 + 2\|\mathbf{a}_m^{\mathscr{A}} - \mathbf{R}\mathbf{s}_i^{\mathscr{B}} - \mathbf{t}\| r_{im} + r_{im}^2 \tag{3b}$$

We subtract σ_{im}^2 from both sides of (3b) and have:

$$d_{im}^2 - \sigma_{im}^2 = \|\mathbf{a}_m^{\mathscr{A}}\|^2 - 2\mathbf{a}_m^{\mathscr{A}\top}(\mathbf{R}\mathbf{s}_i^{\mathscr{B}} + \mathbf{t}) + \|\mathbf{R}\mathbf{s}_i^{\mathscr{B}} + \mathbf{t}\|^2 + e_{im}, \tag{4}$$

where $e_{im} = 2\|\mathbf{a}_m^{\mathscr{A}} - \mathbf{R}\mathbf{s}_i^{\mathscr{B}} - \mathbf{t}\| r_{im} + (r_{im}^2 - \sigma_{im}^2)$ has zero mean.

Stacking (4) over all measurements for i-th tag gives

$$\mathbf{d}_i = -2\mathbf{A}^\top(\mathbf{R}\mathbf{s}_i^{\mathscr{B}} + \mathbf{t}) + \|\mathbf{R}\mathbf{s}_i^{\mathscr{B}} + \mathbf{t}\|^2 \mathbf{1}_{M_T} + \mathbf{e}_i \tag{5}$$

where

$$\mathbf{A} = \begin{bmatrix} \mathbf{a}_1^{\mathscr{A}} & \mathbf{a}_2^{\mathscr{A}} \cdots \mathbf{a}_{M_T}^{\mathscr{A}} \end{bmatrix} \in \mathbb{R}^{2\times M_T} \quad \mathbf{S} = \begin{bmatrix} \mathbf{s}_1^{\mathscr{B}} & \mathbf{s}_2^{\mathscr{B}} \cdots \mathbf{s}_N^{\mathscr{B}} \end{bmatrix} \in \mathbb{R}^{2\times N}$$

$$\mathbf{d_i} = \begin{bmatrix} d_{i1}^2 - \|\mathbf{a}_1^{\mathscr{A}}\|^2 - \sigma_{i1}^2 \\ \vdots \\ d_{iM_T}^2 - \|\mathbf{a}_{M_T}^{\mathscr{A}}\|^2 - \sigma_{iM_T}^2 \end{bmatrix} \quad \text{and} \quad \mathbf{e_i} = \begin{bmatrix} e_{i1} \\ \vdots \\ e_{iM_T} \end{bmatrix}.$$

The squared least squares problem is formulated as follows:

$$\textbf{(SLS)} \ \min_{\mathbf{R},\mathbf{t}} \ \sum_{i=1}^{N} \|\mathbf{d}_i + 2\mathbf{A}^\top(\mathbf{R}\mathbf{s}_i^{\mathscr{B}} + \mathbf{t}) - \|\mathbf{R}\mathbf{s}_i^{\mathscr{B}} + \mathbf{t}\|^2 \mathbf{1}_{M_T}\|_{\Sigma_{\mathbf{e}_i}}^2 \tag{6a}$$

$$\text{s.t.} \quad \mathbf{R} \in \mathrm{SO}(2), \ \mathbf{t} \in \mathbb{R}^2, \tag{6b}$$

where $\|\cdot\|_\Sigma^2 \triangleq (\cdot)^\top \Sigma^{-1}(\cdot)$, and $\Sigma_{\mathbf{e}_i}$ is the covariance of $\mathbf{e}_i$.

III. An Efficient Planar Pose Estimator

We design the planar pose estimator in two steps, grounded on the following theorem:

Theorem 1: Suppose that $\hat{\mathbf{R}}$ and $\hat{\mathbf{t}}$ are $\sqrt{n}$-consistent estimates of $\mathbf{R^o}$ and $\mathbf{t^o}$. The estimates $\hat{\mathbf{R}}_{\mathrm{GN}}, \hat{\mathbf{t}}_{\mathrm{GN}}$ obtained by one step of Gauss-Newton iteration on the ML problem (2) converge in probability to the ML estimates as measurement number n increases, and

$$\hat{\mathbf{R}}_{\mathrm{GN}} - \hat{\mathbf{R}}_{\mathrm{ML}} = o_p(\mathbf{1}/\sqrt{n}), \quad \hat{\mathbf{t}}_{\mathrm{GN}} - \hat{\mathbf{t}}_{\mathrm{ML}} = o_p(\mathbf{1}/\sqrt{n}),$$

The proof is given in the full version of this paper [21].

Remark 3: Theorem 1 motivates us to design an as computationally efficient as possible $\sqrt{n}-$consistent estimator and refine it by one step of Gauss-Newton iteration. We discuss these two steps in section III-A and III-B respectively.

A. Unconstrained Least Squares Estimator

Denote the projection matrix onto $\mathrm{Null}(\mathbf{1_{M_T}})$ as $\mathbf{P} = \mathbf{I}_{M_T} - (\mathbf{1}_{M_T}\mathbf{1}_{M_T}^\top)/M_T$. Multiply both sides of (5) by $\mathbf{P}$ and eliminate the quadratic term, we formulate the following problem [16]:

$$\textbf{(PSLS)} \ \min_{\mathbf{R},\mathbf{t},\mathbf{n}} \ \sum_{i=1}^{N} \|\mathbf{P}\mathbf{d}_i + 2\mathbf{P}\mathbf{A}^\top(\mathbf{R}\mathbf{s}_i^{\mathscr{B}} + \mathbf{t})\|_{\Sigma_{\bar{\mathbf{e}}_i}}^2 \tag{7a}$$

$$\text{s.t.} \quad \mathbf{R} \in \mathrm{SO}(2), \ \mathbf{t} \in \mathbb{R}^2 \tag{7b}$$

where $\Sigma_{\bar{\mathbf{e}}_i}$ is the covariance matrix for $\mathbf{P}\mathbf{e}_i$.

The rotation matrix $\mathbf{R}$ has a nice structure, such that we can parameterize $\mathbf{R}$ by an angle $\theta \in [0, 2\pi)$:

$$\mathbf{R}(\theta) \triangleq \begin{bmatrix} \cos\theta & -\sin\theta \\ \sin\theta & \cos\theta \end{bmatrix}. \tag{8}$$

Motivated by (8), we can use a unit-length vector $\mathbf{y} = (y_1, y_2) \in \mathbb{R}^2$ to parameterize $\mathbf{R}$, where y_1, y_2 correspond to $\sin(\theta), \cos(\theta)$ respectively. Denote $\mathbf{AP}$ as $\bar{\mathbf{A}}$, $\mathbf{P}\mathbf{d}_i$ as $\bar{\mathbf{d}}_\mathbf{i}$, and $\mathbf{P}\mathbf{e}_i$ as $\bar{\mathbf{e}}_\mathbf{i}$, we formulate the following GTRS problem:

$$\min_{\mathbf{y},\mathbf{t}} \ \|\bar{\mathbf{d}} - \mathbf{H}_1\Gamma\mathbf{y} - \mathbf{H}_2\mathbf{t}\|_{\Sigma_{\bar{e}}^{-1}}^2 \quad \text{s.t.} \ \|\mathbf{y}\|^\mathbf{2} = \mathbf{1} \tag{9}$$

where $\Gamma = \begin{bmatrix} 0 & 1 & -1 & 0 \\ 1 & 0 & 0 & 1 \end{bmatrix}^\top$, $\bar{\mathbf{d}} = (\bar{\mathbf{d}}_1, \ldots, \bar{\mathbf{d}}_N)$, $\mathbf{H}_1 = -2\mathbf{S}^\top \otimes \bar{\mathbf{A}}^\top$, and $\mathbf{H}_2 = -2\mathbf{1_N} \otimes \bar{\mathbf{A}}^\top$.

The matrix $\Sigma_{\bar{\mathbf{e}}}$ is dense and dependent on true distance d_{im}^o's [16]. We discard the constraint and covariance for efficiency and simplicity and solve the resultant LS problem.

Lemma 1: Under Assumption 4, the design matrix $\mathbf{H} = [\mathbf{H}_1\Gamma, \mathbf{H_2}]$ is full column rank, and the unique solution to the resultant LS problem is given by:

$$\textbf{(ULS)} \qquad \begin{bmatrix} \hat{\mathbf{y}} \\ \hat{\mathbf{t}} \end{bmatrix} = (\mathbf{H}^\top\mathbf{H})^{-\mathbf{1}}\mathbf{H}^\top\bar{\mathbf{d}}, \tag{10}$$

Theorem 2: The **ULS** estimator is $\sqrt{n}$-consistent, i.e.,

$$\begin{bmatrix} \hat{\mathbf{y}} \\ \hat{\mathbf{t}} \end{bmatrix} - \begin{bmatrix} \mathbf{y}^o \\ \mathbf{t}^o \end{bmatrix} = O_p(\mathbf{1}/\sqrt{n}).$$

The proof is given in the full version of this paper [21].

Notice that the estimate $\hat{\mathbf{y}}$ from (10) is not constrained to have unit length, so we further project $\hat{\mathbf{R}} \triangleq \Gamma\hat{\mathbf{y}}$ onto $\mathrm{SO}(2)$. The matrix projection π that maps an arbitrary matrix $\mathbf{X} \in \mathbb{R}^{2\times 2}$ onto $\mathrm{SO}(2)$ is defined as

$$\pi(\mathbf{X}) = \arg\min_{\mathbf{W}\in\mathrm{SO}(2)} \|\mathbf{X} - \mathbf{W}\|_F^2. \tag{11}$$

Let the SVD of $\mathbf{X}$ be $\mathbf{U}\Sigma\mathbf{V}^\top$, we have

$$\pi(\mathbf{X}) = \mathbf{U}\mathrm{diag}([1, \det(\mathbf{U}\mathbf{V}^\top)])\mathbf{V}^\top \tag{12}$$

Theorem 3: The projected estimate generated by (11) is $\sqrt{n}$-consistent, i.e.,

$$\pi(\hat{\mathbf{R}}) - \mathbf{R}^o = O_p(\mathbf{1}/\sqrt{n}).$$

The proof is given in the full version of this paper [21].

Remark 4: By assigning $O^{\mathscr{B}}$ on tag j, the measurement model of tag i becomes $d_{jm} = \|\mathbf{a}_m^{\mathscr{A}} - \mathbf{t}^o\| + r_{jm}$. We can thus estimate translation $\mathbf{t}^o$ first using d_{jm}'s, and then substitute $\hat{\mathbf{t}}$ to estimate the rotation matrix $\mathbf{R}^o$. Similarly, we can first localize the tags and then infer the pose, as in work [23].

The accuracy of the intermediate step is crucial for such divide-and-conquer schemes. Given a $\sqrt{M_T}-$consistent estimate for the intermediate step, the resultant pose estimator can achieve $\sqrt{n}-$consistency, as shown in section V and proved in the longer version of this paper [21].

B. One Step of the Gauss-Newton Iteration

Given a $\sqrt{n}$-consistent estimate from the first step, we implement one step of Gauss-Newton iteration on the **ML** problem (2) and obtain the **GN-ULS** estimator. Using (8), we can transform problem (2) into an unconstrained one:

$$\min_{\theta,\mathbf{t}} \quad \sum_{i=1}^{N}\sum_{m=1}^{M_T} \frac{(d_{im} - \|\mathbf{a}_m^{\mathscr{A}} - \mathbf{L}_i \mathrm{vec}\left(\mathbf{R}(\hat{\theta}+\theta)\right) - \mathbf{t}\|)^2}{\sigma_{im}^2} \tag{13}$$

where $\mathbf{L}_i = (\mathbf{s}_i^{\mathscr{B}} \otimes \mathbf{I}_2)^\top \in \mathbb{R}^{2\times 4}$ and $\mathbf{R}(\hat{\theta}) = \pi(\hat{\mathbf{R}})$.

We use $\theta = 0, \mathbf{t} = \hat{\mathbf{t}}$ as the initial value. Write $f_{im}(\theta,\mathbf{t}) \triangleq \mathbf{a}_m^{\mathscr{A}} - \mathbf{L}_i \mathrm{vec}\left(\mathbf{R}(\hat{\theta}+\theta)\right) - \mathbf{t}$ and $f_{im}^{(0)} \triangleq f_{im}(0,\hat{\mathbf{t}})$. The derivatives of $\|f_{im}^{(0)}\|$ w.r.t θ and $\mathbf{t}$ are:

$$\frac{\partial \|f_{im}^{(0)}\|}{\partial(\theta,\mathbf{t})} = \begin{bmatrix} -\frac{1}{\|f_{im}^{(0)}\|}\Psi^\top(\mathbf{I}_2 \otimes \hat{\mathbf{R}}^\top)\mathbf{L}_i^\top f_{im}^{(0)} \\ -\frac{1}{\|f_{im}^{(0)}\|} f_{im}^{(0)} \end{bmatrix}$$

where $\Psi = \frac{\partial \mathrm{vec}(\mathbf{R}(0))}{\partial \theta} = \begin{bmatrix} 0 & 1 & -1 & 0 \end{bmatrix}^\top$. Stacking the rows $\frac{\partial \|f_{im}(0,\hat{\mathbf{t}})\|}{\partial(\theta,\mathbf{t})^\top}$ gives the matrix $\mathbf{J}_0$. Stacking $\|f_{im}^{(0)}\|$ gives the vector $\mathbf{f}(0,\hat{\mathbf{t}})$. Denote the covariance matrix of r_{im} as Σ_n, the one step of Gauss-Newton iteration $(\hat{\theta},\hat{\mathbf{t}})_{\mathrm{GN}}$ writes:

$$(\hat{\theta},\hat{\mathbf{t}})_{\mathrm{GN}} = (0,\hat{\mathbf{t}}) + (\mathbf{J}_0^\top \Sigma_n^{-1}\mathbf{J}_0)^{-1}\mathbf{J}_0^\top \Sigma_n^{-1}\left(\mathbf{d} - \mathbf{f}(0,\hat{\mathbf{t}})\right) \tag{14}$$

as such, we obtain the **GN-ULS** estimates,

$$\textbf{(GN-ULS)} \qquad \hat{\mathbf{R}}_{\mathrm{GN}} = \mathbf{R}(\hat{\theta}+\hat{\theta}_{\mathrm{GN}}), \quad \hat{\mathbf{t}}_{\mathrm{GN}} = \hat{\mathbf{t}}_{\mathrm{GN}} \tag{15}$$

We summarize the **GN-ULS** estimator in Algorithm 1.

Algorithm 1 Unconstrained Least Squares estimator refined by one-step of Gauss-Newton iteration (GN-ULS)

Input: d_{im}, σ_{im}, $\mathbf{a}_m^{\mathscr{A}}$ and $\mathbf{s}_i^{\mathscr{B}}$.
Output: the estimates of $\mathbf{R}^o$ and $\mathbf{t}^o$.
1: Construct $\bar{\mathbf{d}} \in \mathbb{R}^{n\times 1}$ and $\mathbf{H} \in \mathbb{R}^{n\times 4}$.
2: Derive the **ULS** estimator as $(\mathbf{H}^\top\mathbf{H})^{-1}\mathbf{H}^\top\bar{\mathbf{d}}$.
3: Project the **ULS** estimate onto $SO(2)$ (11).
4: Construct $\mathbf{J}_0 \in \mathbb{R}^{n\times 3}$ and $\mathbf{f}(0,\hat{\mathbf{t}}) \in \mathbb{R}^{n\times 1}$.
5: Implement one step of Gauss-Netwon iteration (14).
6: Obtain the **GN-ULS** estimator (15).

IV. Statistical Efficiency Analysis

According to Theorem 1, the **GN-ULS** estimates converge to the ML estimates as n increases. The following theorem describes the **GN-ULS** estimator's statistical efficiency.

Theorem 4: Under assumptions 3-5, the **ML** estimates, therefore the **GN-ULS** estimates are asymptotically efficient, i.e., as measurement number n increases,

$$\mathrm{CRLB}^{-1/2}\begin{bmatrix} \mathrm{vec}(\hat{\mathbf{R}}_{\mathrm{ML}} - \mathbf{R}^o) \\ \hat{\mathbf{t}}_{\mathrm{ML}} - \mathbf{t}^o \end{bmatrix} \xrightarrow{D} \mathscr{N}(\mathbf{0},\mathbf{I}),$$

$$\mathrm{CRLB}^{-1/2}\begin{bmatrix} \mathrm{vec}(\hat{\mathbf{R}}_{\mathrm{GN}} - \mathbf{R}^o) \\ \hat{\mathbf{t}}_{\mathrm{GN}} - \mathbf{t}^o \end{bmatrix} \xrightarrow{D} \mathscr{N}(\mathbf{0},\mathbf{I}).$$

The formula for CRLB and proof are detailed in [21].

Remark 5: This theorem establishes the proposed estimator's optimality and legitimates us to approximate estimation covariance by CRLB, which is a vital problem in sensor fusion schemes. Although we need the true pose to calculate CRLB, we can reasonably use $\hat{\mathbf{R}}_{\mathrm{GN}}, \hat{\mathbf{t}}_{\mathrm{GN}}$ as an alternative.

CRLB is related to sensor deployment in a complicated way, making it difficult to design a sensor deployment strategy from the view of theoretical lower bound. But in general, we should deploy the tags as sparsely as possible [21].

V. Simulations and Discussions

We verify the asymptotic efficiency of the proposed **GN-ULS** estimator by comparing the root mean square error (RMSE) with the lower bound, which is the square root of the trace of CRLB [16], denoted as $\sqrt{CRLB}$. We compare with previous works [17] and [18], denoted as the **GTRS** and the **GN-SDP** respectively. We also compare with the divide-and-conquer approach that localizes the tags first. For the implementation of this estimator, denoted as **DAC**, we follow work [24] for localization and solve a least squares problem for pose estimation. Given a $\sqrt{M_T}-$consistent position estimator, this **DAC** estimator can be proved to be $\sqrt{n}-$consistent, detailed in the full version of this paper [21].

A. Simulation Setup

In our simulations, there are $M = 3$ anchors deployed at $[50,0]^\top$, $[50,50]^\top$ and $[0,50]^\top$ in the global frame. There are $N = 2$ tags deployed at $[3,0]^\top$ and $[3,3]^\top$ in the local frame. The true pose is $\mathbf{t}^o = [0,25]^\top$ and $\theta^o = 60^\circ$.

We run $L = 1000$ Monte-Carlo experiments for each setting and report the average results. We use the chordal distance [25] to calculate the RMSE for the rotation matrix:

$$\mathrm{RMSE}(\mathbf{R}) = \sqrt{\frac{1}{L}\sum_{l=1}^{L}\|\hat{\mathbf{R}} - \mathbf{R}^o\|_F^2}$$

B. Simulation Results

1) Asymptotic efficiency under repeated ranging: We increase the number T of repeated ranging. The noise standard deviation σ_{mi}'s are set to be $0.05[1,2,3,4,5,6]$. As shown in Fig. 2a, the **ULS** estimator and the **DAC** estimator are $\sqrt{n}-$consistent but not asymptotically efficient. The **GTRS** estimator deviates from the lower bound under large samples, and the main reason is that the estimate is refined on the **SLS** problem (6) but not on the **ML** problem (2). The **GN-ULS** and the **DAC** estimator are significantly more efficient with $O(n)$ complexity, as shown in Figure. 2b. It also takes $O(n)$ computation to construct the optimization problems for the **GN-ULS** and the **GN-SDP** estimator, but solving the problems dominates the computation cost.

2) Asymptotic efficiency under numerous anchors: We deploy new anchors uniformly on the simulation plane. The standard deviation σ_{im} is set to be 0.1. As shown in Fig. 3a, the **GTRS** estimator deviates from the lower bound. When we deploy 10000 anchors, the MATLAB CVX toolbox reports the SDP problem as infeasible. The same instability problem occurs in Fig. 3b under very small noise.

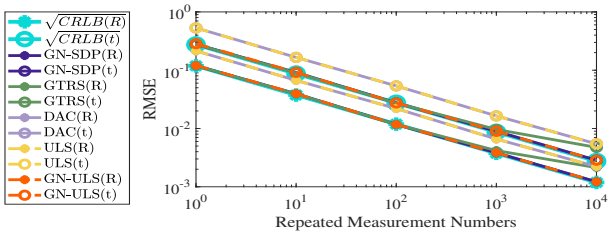

(a)

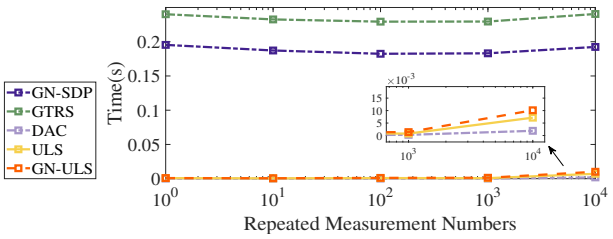

(b)

Fig. 2: Performance under repeated ranging. (a) RMSE of different pose estimators and the lower bound as the number T of repeated ranging increases. (b) Average computation time of different pose estimators as T increases.

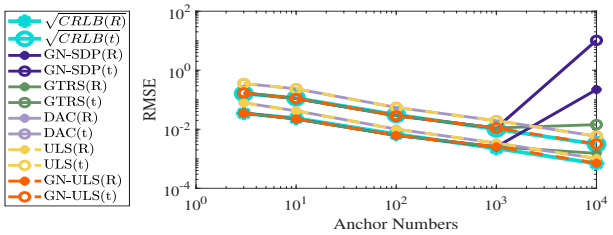

(a)

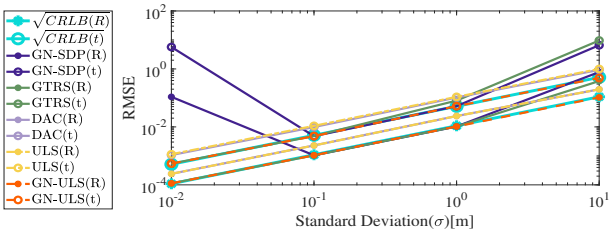

(b)

Fig. 3: Performance with numerous anchors and under different noise levels. (a) RMSE of different pose estimators and the lower bound when the number M of anchors increases. (b) RMSE of different pose estimators and the lower bound as the standard deviation increases.

3) Asymptotic efficiency under large noise: We adjust the standard deviation σ_{im} from 0.01 to 10, and set $T = 1000$. As shown in Fig. 3b, **GTRS** and **GN-SDP** deviate from the lower bound under large nose, this is because they omit r_{im}^2 in (3b) and use noisy measurements to calculate the covariance matrix $\Sigma_{\bar{\mathbf{e}}_i}$.

C. Discussions

As the simulation results indicate, the **GN-ULS** attains theoretical lower bound, and performs better than computationally more complex estimators in stability and accuracy. As guaranteed by Theorem 1, the **DAC** estimator refined by one step of Gauss-Newton can perform comparably well to **GN-ULS**. But the **DAC** estimator appears more sensitive to outliers in dynamic experiments, as shown in Section VI.

VI. Experiments

In this section, we introduce data collection and present experimental results on static and dynamic datasets.

A. System Overview

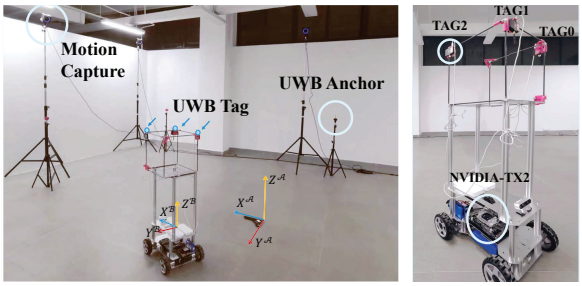

Fig. 4: Experiment Setup

Fig. 4 presents the experimental system and environment with an overall volume of $10m \times 6m \times 4m$. The system consists of a motion capture system (OptiTrack: X22), UWB (NoopLoop: LinkTrack), an Ackerman trolley platform, and an embedded processor (NVIDIA: TX2). We use a carbon fibre cube frame, rather than directly using the trolley, as the rigid body to avoid blocking the UWB signal. Three UWB tags are fixed on the cube at approximately the same height as the eight anchors deployed in the environment.

B. Data Collection

We refer to the motion capture frame as the global frame. The UWB ranging frequency is 100Hz, and the motion capture system provides the ground truth of the pose at 120Hz, with ± 0.15 millimeters and ± 0.5 degrees claimed accuracy[2]. During experiments, NVIDIA-TX2 unpacks the UWB data through its serial port and collects the motion capture system data through TCP. In dynamic datasets, we synchronize measurements using the system time of TX2 and perform interpolation to align the motion capture measurements with the UWB measurements[3]

C. UWB Calibration

UWB ranging measurement is practically modeled as:

$$\hat{d} = d^o + f(d^o) + e, \tag{16}$$

where $f(d^o)$ is a distance-related bias, and e is a zero-mean Gaussian noise. We quiescent the trolley for a period of time and use the sample variance to estimate the standard deviation of e. The more demanding task is calibrating $f(d^o)$, which we assume to be a linear function of d^o [26]. We control the trolley to move around in the environment, collect

[2]https://optitrack.com/cameras/primex-22/

[3]On the dynamic datasets, we observe a positive bias between estimated yaw and the ground truth for all compared methods. We believe this phenomenon is due to imperfect synchronization caused by processing delay and unreliable ground truth for yaw when reflective markers are hidden from some cameras. As a remedy, we compensate all estimates by a negative degree on dynamic datasets.

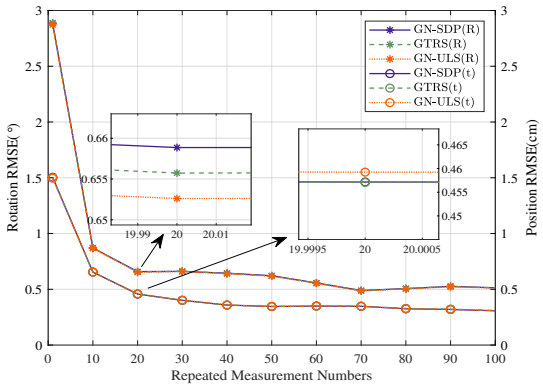

Fig. 5: Static experiment under repeated ranging

calibration datasets and use the least squares method to fit $f(d^o)$. Considering the complex communication environment indoors, we implement outlier rejection before calibration. Similar to the methods in [6], [13], a range measurement at instant t is rejected as an outlier if

$$d_t > \min\{d_{t-k},\ldots,d_{t-1}\} + \frac{kv_{\max}}{f} + 0.1, \qquad (17)$$

where k is the length of the time window, $v_{\max}$ is the velocity upper bound during the experiment, f is the ranging frequency, and $0.1m$ is a general error bound of UWB.

D. Static Datasets and Pose Estimation Results

We place the trolley at 7 different sites and change the orientation from 0° to 300° at an interval of approximately 60°. In total, we collect 42 static datasets, each lasting for around 100 seconds. We calculate the RMSE on all datasets and compare the average result. We choose two tags and three anchors and use the centimeter and the degree as units for Fig. 5. The result shows that all methods achieve similar accuracy to the ground truth system.

E. Dynamic Datasets and Pose Estimation Results

We control the trolley to move at different speeds (0.49m/s, 0.23m/s, and 0.11m/s), and collect fast, medium, and slow datasets. We implement interpolation when an outlier occurs to provide real-time estimates. It is not reasonable to use repeated measurements in the dynamic case. Instead, we adopt all three tags and eight anchors.

Fig. 6 visualizes the results on the fast dataset, where **GN-ULS** achieves an average RMSE of 3.97 degrees and 3.01 centimeters using 24 range measurements between eight anchors and three tags. Overall results on the three datasets are summarized in Table I, where **GN-DAC** represents one step of Gauss-Newton iteration based on the **DAC** estimator.

F. Discussions

All compared methods achieve similar accuracy in the experiments, given the standard deviation of noise in the magnitude of a centimeter. However, the **GN-ULS** and **GN-DAC** estimators significantly reduce the computation time. We attribute this advantage to the insights provided by Theorem 1. We also observe that the **DAC** estimator is less robust to outliers than the **ULS** estimator.

TABLE I: Position and Rotation RMSE on dynamic datasets

Method	Position RMSE [cm]			Rotation RMSE [deg]		
	Fast	Mid	Slow	Fast	Mid	Slow
ULS	3.73	3.55	3.48	5.68	4.74	5.53
DAC	3.60	3.07	3.14	11.55	11.74	11.18
GN-ULS	3.01	3.00	2.59	**3.97**	3.40	**3.75**
GN-DAC	3.07	3.07	2.65	4.39	3.80	4.21
GN-SDP	**3.00**	**3.00**	**2.58**	3.99	**3.37**	3.80
GTRS	3.22	3.27	2.83	4.42	3.97	4.13

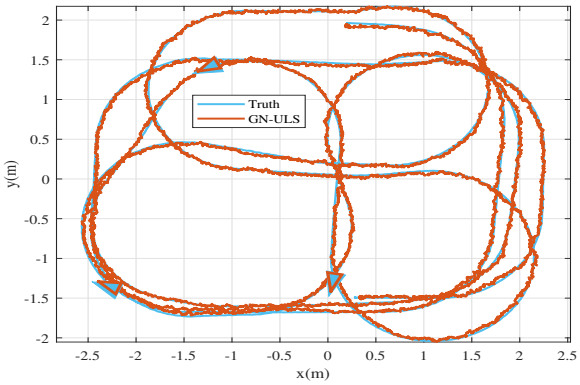

Fig. 6: Dynamic experiment on the fast dataset

The estimators' performance on the dynamic datasets is not as good as on the static datasets. The main reason is the complex indoor environment, where the distance-related bias $f(d^o)$ varies at different positions and orientations due to obstruction and signal reflection from the walls.

VII. Conclusion and Future Work

This work studies planar pose estimation using UWB range measurements. Grounded on a two-step scheme, we design an asymptotically efficient pose estimator **GN-ULS**. The proposed estimator defeats previous works in computational efficiency, stability, and accuracy under large noise. We also find that using a $\sqrt{M_T}-$consistent intermediate estimator, the divide-and-conquer estimation scheme followed by one step of Gauss-Newton iteration performs comparably well but less robust to outliers.

In this work, we intend to present the possibility of using only range measurements for real-time pose estimation. The estimated trajectory is expected to be smoother and more accurate if integrated with motion models or odometry measurements. In future work, we plan to cope with the synchronization problem as the number of tags and sensors increases and the update frequency decreases, which is very important in large-scale dynamic scenarios.

Acknowledgment

This work was supported in part by the National Natural Science Foundation of China under grant no. 62273288, and in part by Shenzhen Science and Technology Program JCYJ20220818103000001. The authors would like to thank Prof Huihuan Qian, Dr. Kaiwen Xue, and Mr. Jiale Zhong from The Chinese University of Hong Kong, Shenzhen, for their help in the experiment conduction.

REFERENCES

[1] J. Zhang and S. Singh, "Low-drift and real-time lidar odometry and mapping," *Autonomous Robots*, vol. 41, no. 2, pp. 401–416, 2017.

[2] W. Zhen and S. Scherer, "Estimating the localizability in tunnel-like environments using lidar and uwb," in *2019 International Conference on Robotics and Automation (ICRA)*. IEEE, 2019, pp. 4903–4908.

[3] T. Shan, B. Englot, D. Meyers, W. Wang, C. Ratti, and D. Rus, "Lio-sam: Tightly-coupled lidar inertial odometry via smoothing and mapping," in *2020 IEEE/RSJ international conference on intelligent robots and systems (IROS)*. IEEE, 2020, pp. 5135–5142.

[4] L. Schmid, D. Salido-Monzú, and A. Wieser, "Accuracy assessment and learned error mitigation of uwb tof ranging," in *2019 International Conference on Indoor Positioning and Indoor Navigation (IPIN)*. IEEE, 2019, pp. 1–8.

[5] J. González, J.-L. Blanco, C. Galindo, A. Ortiz-de Galisteo, J.-A. Fernández-Madrigal, F. A. Moreno, and J. L. Martinez, "Mobile robot localization based on ultra-wide-band ranging: A particle filter approach," *Robotics and autonomous systems*, vol. 57, no. 5, pp. 496–507, 2009.

[6] X. Fang, C. Wang, T.-M. Nguyen, and L. Xie, "Graph optimization approach to range-based localization," *IEEE Transactions on Systems, Man, and Cybernetics: Systems*, vol. 51, no. 11, pp. 6830–6841, 2020.

[7] G. Zeng, B. Mu, J. Wei, W. S. Wong, and J. Wu, "Localizability with range-difference measurements: Numerical computation and error bound analysis," *IEEE/ACM Transactions on Networking*, 2022.

[8] K. Xue, J. Li, N. Xiao, J. Liu, X. Ji, and H. Qian, "Improving the robot localization accuracy using range-only data: An optimization approach," in *2021 6th IEEE International Conference on Advanced Robotics and Mechatronics (ICARM)*. IEEE, 2021, pp. 785–790.

[9] G. Zeng, B. Mu, L. Shi, J. Chen, and J. Wu, "Consistent and asymptotically efficient localization from range-difference measurements," 2023.

[10] Y. Song, M. Guan, W. P. Tay, C. L. Law, and C. Wen, "Uwb/lidar fusion for cooperative range-only slam," in *2019 international conference on robotics and automation (ICRA)*. IEEE, 2019, pp. 6568–6574.

[11] T.-M. Nguyen, M. Cao, S. Yuan, Y. Lyu, T. H. Nguyen, and L. Xie, "Viral-fusion: A visual-inertial-ranging-lidar sensor fusion approach," *IEEE Transactions on Robotics*, vol. 38, no. 2, pp. 958–977, 2021.

[12] C. Wang, H. Zhang, T.-M. Nguyen, and L. Xie, "Ultra-wideband aided fast localization and mapping system," in *2017 IEEE/RSJ international conference on intelligent robots and systems (IROS)*. IEEE, 2017, pp. 1602–1609.

[13] Y. Cao and G. Beltrame, "Vir-slam: Visual, inertial, and ranging slam for single and multi-robot systems," *Autonomous Robots*, vol. 45, no. 6, pp. 905–917, 2021.

[14] J. P. Queralta, J. Taipalmaa, B. Can Pullinen, V. K. Sarker, T. Nguyen Gia, H. Tenhunen, M. Gabbouj, J. Raitoharju, and T. Westerlund, "Collaborative multi-robot search and rescue: Planning, coordination, perception, and active vision," *IEEE Access*, vol. 8, pp. 191 617–191 643, 2020.

[15] H.-Y. Chung, C.-C. Hou, and Y.-S. Chen, "Indoor intelligent mobile robot localization using fuzzy compensation and kalman filter to fuse the data of gyroscope and magnetometer," *IEEE Transactions on Industrial Electronics*, vol. 62, no. 10, pp. 6436–6447, 2015.

[16] S. P. Chepuri, G. Leus, and A.-J. van der Veen, "Rigid body localization using sensor networks," *IEEE Transactions on Signal Processing*, vol. 62, no. 18, pp. 4911–4924, 2014.

[17] S. Chen and K. Ho, "Accurate localization of a rigid body using multiple sensors and landmarks," *IEEE Transactions on Signal Processing*, vol. 63, no. 24, pp. 6459–6472, 2015.

[18] J. Jiang, G. Wang, and K. Ho, "Sensor network-based rigid body localization via semi-definite relaxation using arrival time and doppler measurements," *IEEE Transactions on Wireless Communications*, vol. 18, no. 2, pp. 1011–1025, 2019.

[19] D. M. Rosen, K. J. Doherty, A. Terán Espinoza, and J. J. Leonard, "Advances in inference and representation for simultaneous localization and mapping," *Annual Review of Control, Robotics, and Autonomous Systems*, vol. 4, pp. 215–242, 2021.

[20] B. Großiwindhager, M. Stocker, M. Rath, C. A. Boano, and K. Römer, "Snaploc: An ultra-fast uwb-based indoor localization system for an unlimited number of tags," in *2019 18th ACM/IEEE International Conference on Information Processing in Sensor Networks (IPSN)*. IEEE, 2019, pp. 61–72.

[21] H. Jiang, W. Wang, Y. Shen, X. Li, X. Ren, B. Mu, and J. Wu, "Efficient planar pose estimation via uwb measurements," 2022.

[22] S.-M. Lee, "Ultrawideband (uwb)-based precise short-range localization for wireless power transfer to electric vehicles in parking environments," *PeerJ Computer Science*, vol. 7, p. e567, 2021.

[23] C. Bonsignori, F. Condomitti, M. Del Gamba, F. Garzelli, L. Lossi, F. Mione, A. Noferi, and A. Vecchio, "Estimation of user's orientation via wearable uwb," in *2020 16th International Conference on Intelligent Environments (IE)*. IEEE, 2020, pp. 80–83.

[24] G. Zeng, B. Mu, J. Chen, Z. Shi, and J. Wu, "Global and asymptotically efficient localization from range measurements," *arXiv preprint arXiv:2203.16951*, 2022.

[25] R. Hartley, J. Trumpf, Y. Dai, and H. Li, "Rotation averaging," *International journal of computer vision*, vol. 103, no. 3, pp. 267–305, 2013.

[26] G. Bellusci, G. J. Janssen, J. Yan, and C. C. Tiberius, "Model of distance and bandwidth dependency of toa-based uwb ranging error," in *2008 IEEE International Conference on Ultra-Wideband*, vol. 3. IEEE, 2008, pp. 193–196.